INTERNATIONAL JOURNAL FOR NUMERICAL METHODS IN ENGINEERING
Int. J. Numer. Meth. Engng 2009; **78**:229–252
Published online 10 November 2008 in Wiley InterScience (www.interscience.wiley.com). DOI: 10.1002/nme.2486

An efficient finite element method for embedded interface problems

John Dolbow[1,*,†] and Isaac Harari[2,‡]

[1]*Department of Civil and Environmental Engineering, Duke University, Durham, NC 27708, U.S.A.*
[2]*Faculty of Engineering, Tel Aviv University, 69978 Ramat Aviv, Israel*

SUMMARY

A stabilized finite element method based on the Nitsche technique for enforcing constraints leads to an efficient computational procedure for embedded interface problems. We consider cases in which the jump of a field across the interface is given, as well as cases in which the primary field on the interface is given. The finite element mesh need not be aligned with the interface geometry. We present closed-form analytical expressions for interfacial stabilization terms and simple procedures for accurate flux evaluations. Representative numerical examples demonstrate the effectiveness of the proposed methodology. Copyright © 2008 John Wiley & Sons, Ltd.

Received 3 August 2008; Revised 11 September 2008; Accepted 12 September 2008

KEY WORDS: embedded interface; Nitsche; finite element; stabilization

1. INTRODUCTION

Recently, much attention has focused on the development of finite element methods for embedded interfaces. By embedded, we refer here to those methods in which the finite element mesh is not aligned with the interface geometry. Examples include the extended finite element method (X-FEM) [1, 2], the unfitted finite element methods [3], and the recent immersed finite element method [4]. Such approaches facilitate the treatment of both stationary interfaces with complex geometry and interfaces whose geometry evolves. Pertinent applications range from the modeling of composites with complex microstructure [5] to simulating multi-phase flow [6–9] and biofilm growth [10]. In this work, we present a stabilized finite element method for embedded interfaces,

*Correspondence to: John Dolbow, Department of Civil and Environmental Engineering, Duke University, Box 90287, Durham, NC 27708-0287, U.S.A.
†E-mail: jdolbow@duke.edu
‡This work was done while the author was visiting Duke University.

Contract/grant sponsor: Air Force Office of Scientific Research; contract/grant number: 184592

characterized by the use of Nitsche's method [11] to enforce constraints, closed-form analytical expressions for interfacial stabilization terms, and simple flux evaluations. We focus attention on steady problems, but contend that the techniques and approach are nonetheless well suited to time-dependent problems.

Many interface problems can be roughly classified as falling into one of two categories. From a weighted-residual perspective, the easiest class of interfacial problems concerns those in which the jump in the bulk primary (e.g. displacement, temperature) and/or secondary (e.g. traction, heat flux) field across the interface is known or given. We refer to these as 'jump' problems. A simple example concerns perfectly bonded material interfaces in composites, where both the jump in displacement and normal traction across the interface vanish. The challenge with this class of problems often amounts to capturing the presence of slope discontinuities that arise due to the mismatch in material properties. The X-FEM, for example, can effect this through enrichment with the 'ridge' function developed by Moës *et al.* [5]. Other approaches to material interface problems require the use of blending to properly ramp down the enrichment function (see, e.g. the recent work of Gracie *et al.* [12] or Fries [13], and references contained therein). In this work, we consider the slightly more general case of a non-zero jump in the primary and/or secondary field across the interface. We contend that our approach is both more efficient than the use of ridge enrichment and simpler to implement than blending.

The second class of problems are those in which the primary field on the interface is given. We refer to these as 'Dirichlet' problems. An example includes Gibbs–Thomson conditions arising in crystal growth and solidification problems, where the interfacial temperature is a function of the interfacial velocity and curvature. This class of problems has proven more difficult for embedded methods to address, as standard methods for the weak imposition of constraints have proven insufficient. As shown in Ji and Dolbow [14] and Moës *et al.* [15], for low-order elements the most convenient choice of Lagrange multiplier is unstable. Two different approaches to the issue have emerged: the development of a stable Lagrange multiplier [15] and methods based on stabilizing the convenient choice [16, 17]. This work continues the development of stabilized approaches based on Nitsche's method, including the important derivation of analytical expressions for element-level stabilization parameters.

Dirichlet problems are often complicated by the need for accurate and robust techniques to evaluate the jump in interfacial flux quantities, particularly for evolving interface problems. For example, in many Stefan problems, the normal velocity of the interface is proportional to the jump in flux. Techniques such as penalty methods that may be adequate for enforcing constraints on stationary interfaces often prove to be lacking when it comes to yielding accurate, consistent flux quantities. Here, we revisit our earlier work on domain-integral methods [14], in particular focusing on the ease of implementation and the robustness that is available when combined with a stabilized method.

Our approach shares many common features with the pioneering work of Hansbo and Hansbo [3], particularly the use of Nitsche's method to enforce interfacial constraints in a stable manner. By the same token, there are important differences that bear emphasis. From the outset, we consider a broader class of interfacial problems as constituted by the jump and Dirichlet problems, and provide closed-form analytical expressions for the associated stabilization terms. Particular emphasis is also placed on the extraction of the jump in interfacial flux for Dirichlet problems, an important factor in the robust simulation of evolving interfaces with embedded methods.

This paper is organized as follows. In the following section, we describe the boundary-value problems of interest and the variational forms for two basic types of interfacial conditions. Section 3

DOI: 10.1002/nme

presents the discretization scheme for the bulk and interfacial terms, as well as the domain integral. Section 4 then outlines a method to identify suitable stabilization terms through numerical analysis. Representative numerical examples that test the efficacy of the method are provided in Section 5. Finally, a summary and concluding remarks are provided in the last section.

2. PROBLEM FORMULATION

Consider the problem described by an interface $\mathcal{S}$ partitioning the domain $\mathcal{R}$ into the disjoint sets $\mathcal{R}^+$ and $\mathcal{R}^-$, as shown in Figure 1.

In the bulk regions away from the interface, we consider the governing equation

$$-\nabla\cdot(\kappa\nabla u)+\beta u = f \quad \text{in } \mathcal{R}^+\cup\mathcal{R}^- \tag{1a}$$

$$u = d \quad \text{on } \partial\mathcal{R}_d \tag{1b}$$

$$\kappa\nabla u\cdot\mathbf{n}_o = m \quad \text{on } \partial\mathcal{R}_n \tag{1c}$$

where ∇ is the gradient operator, and $\kappa>0$, $\beta>0$ and f are taken as given scalar fields that may be discontinuous across the interface. The disjoint sets $\partial\mathcal{R}_d$ and $\partial\mathcal{R}_n$ are such that $\overline{\partial\mathcal{R}_d\cup\partial\mathcal{R}_n}=\partial\mathcal{R}$, and $\mathbf{n}_o$ is the outward unit normal to $\partial\mathcal{R}$, as shown in Figure 1. The boundary data d and m are also assumed to be given quantities.

For conditions on the interface, we will consider two basic cases:

$$\text{Jump conditions:} \quad [\![u]\!]=\bar{i}, \quad [\![\kappa\nabla u]\!]\cdot\mathbf{n}=\bar{j} \quad \text{on } \mathcal{S} \tag{2a}$$

or

$$\text{Dirichlet conditions:} \quad u^+=g^+, \quad u^-=g^- \quad \text{on } \mathcal{S} \tag{2b}$$

with $\bar{i}$, $\bar{j}$, and g^+, g^- assumed to be sufficiently smooth functions of position on the interface, and $[\![u]\!]=u^+-u^-$ the jump operator. Here, we use u^+ and u^- to denote the limiting values of the field u as the interface is approached from either $\mathcal{R}^+$ or $\mathcal{R}^-$, respectively.

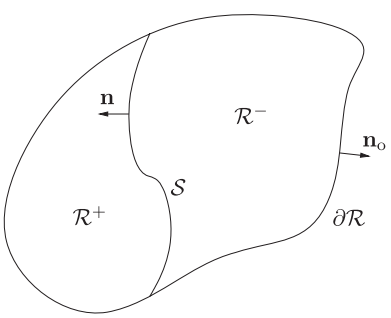

Figure 1. Notation for the two-sided problem. A domain $\mathcal{R}$ partitioned into regions $\mathcal{R}^+$ and $\mathcal{R}^-$ by the interface $\mathcal{S}$. The normal to the interface, $\mathbf{n}$, is defined such that it points outward from the $\mathcal{R}^-$ subdomain, as shown.

DOI: 10.1002/nme

Depending on the choice of parameters, the boundary-value problems given by (1) and (2) represent simplified versions of classical elliptic interface problems. Jump conditions correspond to problems in which both the jump $\bar{\mathrm{i}}$ in the bulk field u and the jump $\bar{\mathrm{j}}$ in the flux across the interface are given. Dirichlet conditions essentially provide the limiting value of the bulk field u as approached from either side of the interface, with g^+, g^- given. With Dirichlet conditions, the jump j in interfacial flux is generally unknown in advance, and represents a quantity of interest. For example, in many Stefan problems, the normal velocity of the interface is proportional to the jump in interfacial flux.

2.1. Variational formulation

The variational form consists of parts associated with bulk and interfacial terms. We write this in a general form as: Find $u \in \mathcal{U}$ such that

$$a_b(v,u)+a_i(v,u)=l_b(v)+l_i(v) \tag{3}$$

for all $v \in \mathcal{V}$. Here, the standard bulk contributions are

$$a_b(v,u) = \int_{\mathcal{R}} (\nabla v \cdot \kappa \nabla u + v\beta u)\,\mathrm{d}\Omega \tag{4a}$$

$$l_b(v) = \int_{\mathcal{R}} vf\,\mathrm{d}\Omega + \int_{\partial\mathcal{R}_n} vm\,\mathrm{d}\Gamma \tag{4b}$$

and the interfacial terms depend on the particular case considered. The solution and weighting spaces are

$$\mathcal{U} = \{u | u \in H^1(\mathcal{R}^- \cup \mathcal{R}^+),\ u = d \text{ on } \partial\mathcal{R}_d\} \tag{5a}$$

$$\mathcal{V} = \{v | v \in H^1(\mathcal{R}^- \cup \mathcal{R}^+),\ v = 0 \text{ on } \partial\mathcal{R}_d\} \tag{5b}$$

with the usual norms.

In our method, interfacial conditions are enforced weakly with Nitsche's method [11]. With Jump conditions (2a) on the interface we have

$$a_i(v,u) = -\int_{\mathcal{S}} [\![v]\!]\langle \kappa \nabla u \cdot \mathbf{n}\rangle\,\mathrm{d}\Gamma - \int_{\mathcal{S}} \langle \kappa \nabla v \cdot \mathbf{n}\rangle [\![u]\!]\,\mathrm{d}\Gamma + \int_{\mathcal{S}} \alpha [\![v]\!][\![u]\!]\,\mathrm{d}\Gamma \tag{6a}$$

$$l_i(v) = \int_{\mathcal{S}} \alpha [\![v]\!]\bar{\mathrm{i}}\,\mathrm{d}\Gamma - \int_{\mathcal{S}} \langle \kappa \nabla v \cdot \mathbf{n}\rangle \bar{\mathrm{i}}\,\mathrm{d}\Gamma + \int_{\mathcal{S}} \langle v\rangle\ \bar{\mathrm{j}}\,\mathrm{d}\Gamma \tag{6b}$$

for the interfacial contributions to the variational form. Here, $\langle\cdot\rangle$ denotes the average quantity on the interface, such that $\langle u\rangle = \frac{1}{2}(u^+ + u^-)$.

We approach problems with Dirichlet conditions (2b) as two 'one-sided' problems. Hence, we write

$$a_i(v,u) = a_i(v,u)^+ + a_i(v,u)^- \tag{7a}$$

$$l_i(v) = l_i(v)^+ + l_i(v)^- \tag{7b}$$

DOI: 10.1002/nme

with

$$a_i(v,u)^+ = \int_{\mathcal{S}} v\kappa^+ \nabla u \cdot \mathbf{n}\,\mathrm{d}\Gamma + \int_{\mathcal{S}} \kappa^+ \nabla v \cdot \mathbf{n} u\,\mathrm{d}\Gamma + \int_{\mathcal{S}} \alpha^+ vu\,\mathrm{d}\Gamma \tag{8a}$$

$$l_i(v)^+ = \int_{\mathcal{S}} \alpha^+ v g^+\,\mathrm{d}\Gamma + \int_{\mathcal{S}} \kappa^+ \nabla v \cdot \mathbf{n} g^+\,\mathrm{d}\Gamma \tag{8b}$$

and

$$a_i(v,u)^- = -\int_{\mathcal{S}} v\kappa^- \nabla u \cdot \mathbf{n}\,\mathrm{d}\Gamma - \int_{\mathcal{S}} \kappa^- \nabla v \cdot \mathbf{n} u\,\mathrm{d}\Gamma + \int_{\mathcal{S}} \alpha^- vu\,\mathrm{d}\Gamma \tag{9a}$$

$$l_i(v)^- = \int_{\mathcal{S}} \alpha^- v g^-\,\mathrm{d}\Gamma - \int_{\mathcal{S}} \kappa^- \nabla v \cdot \mathbf{n} g^-\,\mathrm{d}\Gamma \tag{9b}$$

The difference in signs in certain terms being attributable to the choice of the interfacial normal $\mathbf{n}$ as pointing outward from $\mathcal{R}^-$.

In (5), (7), and (8), there appear stabilization terms employing the parameters α, α^+, and α^-. In the method we propose, the parameters follow from numerical analysis of the discrete form. This is detailed in Section 4. This approach is contrasted with our earlier work employing bubbles [16] and residual-free bubbles [17] to identify stabilization parameters. The use of numerical analysis results in a much more efficient and robust approach, as examined in Section 5.

2.2. Domain integral for flux evaluation

We describe a technique to approximate the jump j in interfacial flux at some point $\mathbf{x}_\mathrm{d}$ on the interface, for Dirichlet conditions. The approach is based on the domain-integral formulation of Ji and Dolbow [14], which may be viewed as a generalization of the boundary flux calculator developed by Carey *et al.* [18].

Consider a weight function v_d with compact support on $\mathcal{R}$, sufficiently smooth, and covering $\mathbf{x}_\mathrm{d}$. We denote the support of v_d by $\mathcal{B} = \mathrm{supp}(v_\mathrm{d})$ and use $\mathcal{B}^+$ and $\mathcal{B}^-$ to denote the intersection of $\mathcal{B}$ with $\mathcal{R}^+$ and $\mathcal{R}^-$, respectively, and $\mathcal{L} = \mathcal{B} \cap \mathcal{S}$ to denote the portion of the interface that lies within $\mathcal{B}$.

Upon multiplying (1a) by v_d and integrating by parts over $\mathcal{B}$, we obtain

$$\int_{\mathcal{L}} v_\mathrm{d} \mathrm{j}\,\mathrm{d}\Gamma = \int_{\mathcal{B}} v_\mathrm{d} f\,\mathrm{d}\Omega + \int_{\partial\mathcal{R}_n} v_\mathrm{d} m\,\mathrm{d}\Gamma - \int_{\mathcal{B}} v_\mathrm{d} \beta u\,\mathrm{d}\Omega - \int_{\mathcal{B}} \nabla v_\mathrm{d} \kappa \nabla u\,\mathrm{d}\Omega \tag{10}$$

where we have used $\mathrm{j} = [\![\kappa \nabla u]\!] \cdot \mathbf{n}$. Given a bulk field u, this can be used to approximate the jump in flux across the portion $\mathcal{L}$ of the interface. Details of the discretization are provided in Section 3.2.

3. DISCRETIZATION

3.1. Discretization of bulk and interfacial terms

We consider a quasi-uniform partition $\mathcal{T}^h$ of the domain $\mathcal{R}$ into non-overlapping element domains $\mathcal{T}_e$ with boundaries $\partial\mathcal{T}_e$. We write $\mathcal{S}^h$ for a partition of the interface $\mathcal{S}$ into a set of non-overlapping segments $\mathcal{S}_e$ taking a particular structure; namely, the vertex set for $\mathcal{S}^h$ is taken as the set of intersection points between $\mathcal{S}$ and the set of element edges $\{\partial\mathcal{T}_e\}$. We consider an 'unfitted' or

DOI: 10.1002/nme

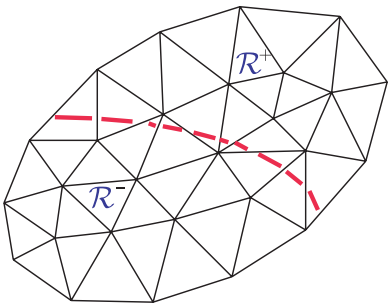

Figure 2. Two-dimensional example of a bulk partition of the domain into a finite element mesh and corresponding partition of the interface.

'embedded' interface method in the sense that no further assumption concerning the structure of the partition $\mathcal{T}^h$ and the interface partition $\mathcal{S}^h$ is made. For the sake of concreteness, an example of $\mathcal{T}^h$ and $\mathcal{S}^h$ is shown in Figure 2.

We follow the usual Galerkin method and consider (3) in terms of finite-dimensional solution $\mathcal{U}^h \subset \mathcal{U}$ and weighting $\mathcal{V}^h \subset \mathcal{V}$ spaces. The Galerkin approximation is given by: Find $u^h \in \mathcal{U}^h$ such that

$$a_b(v^h, u^h) + a_i(v^h, u^h) = l_b(v^h) + l_i(v^h) \tag{11}$$

for all $v^h \in \mathcal{V}^h$.

We write I^+ to denote the set of nodes with basis functions N_I whose supports intersect $\mathcal{R}^+$, i.e.

$$I^+ = \{I : \text{supp}(N_I) \cap \mathcal{R}^+ \neq \emptyset\} \tag{12}$$

and likewise

$$I^- = \{I : \text{supp}(N_I) \cap \mathcal{R}^- \neq \emptyset\} \tag{13}$$

and note that $I^+ \cap I^- \neq \emptyset$. The approximation u^h to the bulk field u is then given by

$$u^h(\mathbf{x}) = \sum_{I \in I^+} N_I(\mathbf{x}) u_I^+ + \sum_{I \in I^-} N_I(\mathbf{x}) u_I^- \tag{14}$$

with u_I^+ and u_I^- denoting degrees-of-freedom. An analogous expansion is employed for the approximation v^h to the weight function v, i.e.

$$v^h(\mathbf{x}) = \sum_{I \in I^+} N_I(\mathbf{x}) v_I^+ + \sum_{I \in I^-} N_I(\mathbf{x}) v_I^- \tag{15}$$

with v_I^+ and v_I^- denoting arbitrary variations.

Remarks

1. The basis for u^h resulting from (14) is identical to an enriched approximation using the X-FEM (see Areias and Belytschko [19]), i.e.

$$u^h(\mathbf{x}) = \sum_I N_I(\mathbf{x}) u_I + \sum_J N_J(\mathbf{x}) H(\mathbf{x}) e_J$$

DOI: 10.1002/nme

where J denotes the set of basis functions whose supports intersect the interface and H is a generalized Heaviside function. Additional details can be found in Song *et al.* [20].
2. Such a construction follows the partition-of-unity framework developed by Melenk and Babuška [21].
3. The approximation (14) can be viewed as one that results from two distinct meshes that happen to possess overlapping elements about the interface.
4. Alternatively, the approximation (14) can be viewed as the finite element analog to the ghost fluid method (see, for example, Liu *et al.* [22]).

Upon substituting (14) and (15) into (11) and invoking the arbitrariness of v^h, we obtain a system of linear algebraic equations that can be written in the form:

$$\begin{bmatrix} \mathbf{K}_{\mathrm{b}}^{+}+\mathbf{K}_{\mathrm{n}}^{+}+\mathbf{K}_{\mathrm{s}}^{+} & \mathbf{K}_{\mathrm{c}} \\ \mathbf{K}_{\mathrm{c}}^{\top} & \mathbf{K}_{\mathrm{b}}^{-}+\mathbf{K}_{\mathrm{n}}^{-}+\mathbf{K}_{\mathrm{s}}^{-} \end{bmatrix} \begin{bmatrix} \mathbf{d}^{+} \\ \mathbf{d}^{-} \end{bmatrix} = \begin{bmatrix} \mathbf{f}_{\mathrm{b}}^{+}+\mathbf{f}_{\mathrm{n}}^{+}+\mathbf{f}_{\mathrm{s}}^{+}+\mathbf{f}_{\mathrm{j}}^{+} \\ \mathbf{f}_{\mathrm{b}}^{-}+\mathbf{f}_{\mathrm{n}}^{-}+\mathbf{f}_{\mathrm{s}}^{-}+\mathbf{f}_{\mathrm{j}}^{-} \end{bmatrix} \tag{16}$$

where $\mathbf{d}^{+}$ and $\mathbf{d}^{-}$ are vectors collecting all degrees-of-freedom u_I^{+} and u_I^{-}, respectively. The stiffness terms are assembled in the usual manner from element contributions. The bulk stiffness terms $\mathbf{K}_{\mathrm{b}}^{+}$ and $\mathbf{K}_{\mathrm{b}}^{-}$ are given by

$$[\mathbf{K}_{\mathrm{b}}^{\pm}]_{IJ} = \sum_e \int_{\mathcal{T}_e^{\pm}} (\nabla N_I \cdot \kappa^{\pm} \nabla N_J + N_I \beta^{\pm} N_J)\, \mathrm{d}\Omega_e \tag{17}$$

where $\mathcal{T}_e^{+}$, $\mathcal{T}_e^{-}$ denote the portion of the element residing in either $\mathcal{R}^{+}$ or $\mathcal{R}^{-}$, respectively. The bulk forcing terms are given by

$$[\mathbf{f}_{\mathrm{b}}^{\pm}]_I = \sum_e \int_{\mathcal{T}_e^{\pm}} N_I f\, \mathrm{d}\Omega_e + \sum_e \int_{\partial\mathcal{T}_{ne}^{\pm}} N_I m\, \mathrm{d}\Gamma_e \tag{18}$$

where $\partial\mathcal{T}_{\mathrm{ne}}$ denotes the portion of the element boundary intersecting the Neumann boundary $\partial\mathcal{R}_{\mathrm{n}}$. The remaining contributions to the stiffness matrix and forcing vector depend on whether the interfacial conditions are of Jump or Dirichlet type.

Jump conditions: The terms follow from the Galerkin approximation to (6b). The Nitsche contributions to the stiffness matrix are

$$[\mathbf{K}_{\mathrm{n}}^{\pm}]_{IJ} = -\frac{1}{2}\sum_e \int_{\mathcal{S}_e} N_I (\kappa^{\pm} \nabla N_J \cdot \mathbf{n})\, \mathrm{d}\Gamma_e - \frac{1}{2}\sum_e \int_{\mathcal{S}_e} N_J (\kappa^{\pm} \nabla N_I \cdot \mathbf{n})\, \mathrm{d}\Gamma_e \tag{19}$$

and the Nitsche contributions to the forcing vector are

$$[\mathbf{f}_{\mathrm{n}}^{\pm}]_I = -\frac{1}{2}\sum_e \int_{\mathcal{S}_e} (\kappa^{\pm} \nabla N_I \cdot \mathbf{n}) \bar{\mathrm{i}}\, \mathrm{d}\Gamma_e \tag{20}$$

The stabilization contributions to the stiffness matrix for Jump condition problems are given by

$$[\mathbf{K}_{\mathrm{s}}^{\pm}]_{IJ} = \sum_e \int_{\mathcal{S}_e} \alpha N_I N_J\, \mathrm{d}\Gamma_e \tag{21}$$

DOI: 10.1002/nme

An algebraic expression for α is provided in Section 4. The stabilization contributions to the forcing vector are given by

$$[\mathbf{f}_{\mathrm{s}}^{+}]_I = \sum_e \int_{\mathcal{S}_e} \alpha N_I \bar{\mathrm{i}} \, \mathrm{d}\Gamma_e \tag{22a}$$

$$[\mathbf{f}_{\mathrm{s}}^{-}]_I = -\sum_e \int_{\mathcal{S}_e} \alpha N_I \bar{\mathrm{i}} \, \mathrm{d}\Gamma_e \tag{22b}$$

The coupling contribution $\mathbf{K}_{\mathrm{c}}$ to the stiffness matrix is given by

$$[\mathbf{K}_{\mathrm{c}}]_{IJ} = -\sum_e \int_{\mathcal{S}_e} \alpha N_I N_J \, \mathrm{d}\Gamma_e - \frac{1}{2} \sum_e \int_{\mathcal{S}_e} \alpha N_I (\kappa^{+} \nabla N_J \cdot \mathbf{n}) \, \mathrm{d}\Gamma_e$$
$$- \frac{1}{2} \sum_e \int_{\mathcal{S}_e} \alpha N_J (\kappa^{-} \nabla N_I \cdot \mathbf{n}) \, \mathrm{d}\Gamma_e \tag{23}$$

Finally, the forcing terms corresponding to the jump in interfacial flux are

$$[\mathbf{f}_{\mathrm{j}}^{\pm}]_I = \frac{1}{2} \sum_e \int_{\mathcal{S}_e} N_I \bar{\mathrm{j}} \, \mathrm{d}\Gamma_e \tag{24}$$

Dirichlet conditions: The terms follow from the Galerkin approximation to (8b) and (9b). The Nitsche contributions to the stiffness matrix are

$$[\mathbf{K}_{\mathrm{n}}^{+}]_{IJ} = \sum_e \int_{\mathcal{S}_e} N_I (\kappa^{+} \nabla N_J \cdot \mathbf{n}) \, \mathrm{d}\Gamma_e + \sum_e \int_{\mathcal{S}_e} N_J (\kappa^{+} \nabla N_I \cdot \mathbf{n}) \, \mathrm{d}\Gamma_e \tag{25a}$$

$$[\mathbf{K}_{\mathrm{n}}^{-}]_{IJ} = -\sum_e \int_{\mathcal{S}_e} N_I (\kappa^{-} \nabla N_J \cdot \mathbf{n}) \, \mathrm{d}\Gamma_e - \sum_e \int_{\mathcal{S}_e} N_J (\kappa^{-} \nabla N_I \cdot \mathbf{n}) \, \mathrm{d}\Gamma_e \tag{25b}$$

and the Nitsche contributions to the forcing vector are

$$[\mathbf{f}_{\mathrm{n}}^{+}]_I = \sum_e \int_{\mathcal{S}_e} (\kappa^{+} \nabla N_I \cdot \mathbf{n}) g^{+} \, \mathrm{d}\Gamma_e \tag{26a}$$

$$[\mathbf{f}_{\mathrm{n}}^{-}]_I = -\sum_e \int_{\mathcal{S}_e} (\kappa^{-} \nabla N_I \cdot \mathbf{n}) g^{-} \, \mathrm{d}\Gamma_e \tag{26b}$$

The stabilization contributions to the stiffness matrix and forcing vector are identical, modulo the use of either α^{+} or α^{-}:

$$[\mathbf{K}_{\mathrm{s}}^{\pm}]_{IJ} = \sum_e \int_{\mathcal{S}_e} \alpha^{\pm} N_I N_J \, \mathrm{d}\Gamma_e \tag{27a}$$

$$[\mathbf{f}_{\mathrm{s}}^{\pm}]_I = \sum_e \int_{\mathcal{S}_e} \alpha^{\pm} N_I g^{\pm} \, \mathrm{d}\Gamma_e \tag{27b}$$

The coupling matrix $\mathbf{K}_{\mathrm{c}}$ vanishes for problems with Dirichlet conditions, as do the forcing terms due to the jump in flux, $\mathbf{f}_{\mathrm{j}}^{+}$ and $\mathbf{f}_{\mathrm{j}}^{-}$.

We note that for elements intersected by an interface segment $\mathcal{S}_e$, the standard element quadrature routines must be modified to account for bulk terms that are active over only a portion of the domain, i.e. $\mathcal{T}_e^{+}$ or $\mathcal{T}_e^{-}$. We follow the procedures outlined in Moës *et al.* [1] that partition elements into sets of subelements for integration purposes.

DOI: 10.1002/nme

3.2. Discretization of domain integral

We consider a discrete form of (10), namely:

$$\int_{\mathcal{S}^h} v_{\mathrm{d}}^h \mathrm{j}^h \,\mathrm{d}\Gamma = \int_{\mathcal{B}^h} v_{\mathrm{d}}^h f \,\mathrm{d}\Omega + \int_{\partial\mathcal{R}_n} v_{\mathrm{d}}^h m \,\mathrm{d}\Gamma - \int_{\mathcal{B}^h} v_{\mathrm{d}}^h \beta u^h \,\mathrm{d}\Omega - \int_{\mathcal{B}^h} \nabla v_{\mathrm{d}}^h \kappa \nabla u^h \,\mathrm{d}\Omega \tag{28}$$

Consider the set of nodes D whose supports intersect the interface $\mathcal{S}^h$:

$$D = \{I : \mathrm{supp}(N_I) \cap \mathcal{S}^h \neq \emptyset\} \tag{29}$$

We employ this set as a basis for both the approximation j^h to the interfacial flux and the domain-integral weight function v_{d} in (10). Hence, we can write

$$\mathrm{j}^h(\mathbf{x}) = \sum_{I \in D} N_I(\mathbf{x}) \mathrm{j}_I, \quad \mathbf{x} \in \mathcal{S}^h \tag{30}$$

where the degrees-of-freedom j_I are to be determined.

Substituting the approximations for j and v_{d} into (28) and invoking the arbitrariness of the weight function, we obtain the linear algebraic system of equations

$$\begin{aligned}
&\sum_e \int_{\mathcal{S}_e} N_I \left(\sum_{J \in D} N_J(\mathbf{x}) \mathrm{j}_J, \right) \mathrm{d}\Gamma \\
&= \sum_e \int_{\mathcal{T}_e^+ \cup \mathcal{T}_e^-} N_I f \,\mathrm{d}\Omega_e + \sum_e \int_{\partial\mathcal{T}_{ne}^+ \cup \partial\mathcal{T}_{ne}^-} N_I m \,\mathrm{d}\Gamma_e \\
&\quad - \sum_e \int_{\mathcal{T}_e} \sum_{J \in D} (\nabla N_I \cdot \kappa^+ \nabla N_J + N_I \beta^+ N_J) u_J^+ \,\mathrm{d}\Omega_e \\
&\quad - \sum_e \int_{\mathcal{T}_e} \sum_{J \in D} (\nabla N_I \cdot \kappa^- \nabla N_J + N_I \beta^- N_J) u_J^- \,\mathrm{d}\Omega_e \quad \forall I \in D
\end{aligned} \tag{31}$$

Conveniently, each of the terms on the right of the above equation can be determined from components of the linear algebraic system (16). Indeed, we can rewrite (31) as

$$\mathbf{M}_{\mathrm{d}} \mathbf{j} = \mathbf{f}_{\mathrm{b}}^+ + \mathbf{f}_{\mathrm{b}}^- - \mathbf{K}_{\mathrm{b}}^+ \mathbf{d}^+ - \mathbf{K}_{\mathrm{b}}^- \mathbf{d}^- \tag{32}$$

where $\mathbf{j}$ is a vector gathering the degrees-of-freedom j_J, and with the understanding that only those rows $I \in D$ from the global system are required.

Employing a lumped-mass approximation to $\mathbf{M}_{\mathrm{d}}$ and assuming the partition-of-unity $\sum_I N_I = 1$, (32) simplifies to

$$\mathrm{j}_I = \frac{1}{\int_{\mathcal{S}_e} N_I \,\mathrm{d}\Gamma_e} [\mathbf{f}_{\mathrm{b}}^+ + \mathbf{f}_{\mathrm{b}}^- - \mathbf{K}_{\mathrm{b}}^+ \mathbf{d}^+ - \mathbf{K}_{\mathrm{b}}^- \mathbf{d}^-] \quad \forall I \in D \tag{33}$$

As a result, once $\mathbf{d}^+$ and $\mathbf{d}^-$ have been determined from (16), a simple post-processing step yields nodal fluxes $\{\mathrm{j}_I\}$ that can be used to approximate the jump in interfacial flux through (30).

DOI: 10.1002/nme

4. ANALYSIS

The method parameters are defined so that the appropriate bilinear form is coercive. This can be done by global considerations [17], but the following local approach offers added simplicity and efficiency.

In the following subsections, we use $a(u^h, v^h)$ to refer to the discrete bilinear form containing both bulk and interfacial components, i.e.

$$a(u^h, v^h) = a_b(u^h, v^h) + a_i(u^h, v^h) \tag{34}$$

and use $a(u^h, v^h)_e$ to denote the restriction to a single element. For convenience, we define an 'energy' norm

$$\|v^h\|_\kappa^2 = (\nabla v, \kappa \nabla v) \tag{35}$$

Here, $(\cdot, \cdot)$ is the L_2 inner product. The duality pairing $\langle \cdot, \cdot \rangle$ denotes integration along the interface.

4.1. Dirichlet condition

As noted, problems with Dirichlet conditions (2b) can be thought of as two 'one-sided' problems. Consider the problem in $\mathcal{R}^-$ only.

We make use of a generalized inverse estimate, that there exists a configuration-dependent constant $C_\mathrm{I} > 0$ such that

$$\|\kappa v^h_{,n}\|_{\mathcal{S}_e} \leqslant C_\mathrm{I} \|v^h\|_{\mathcal{T}_e^-, \kappa} \tag{36}$$

Remark
Similar inequalities appear in the literature [23, 24].

A lower bound of the constant C_I can be estimated for various elements:

- *Linear triangle.* The gradient is constant within the element and the normal derivative is constant along the interface. Assuming that κ is constant within each element

$$\|\kappa v^h_{,n}\|^2_{\mathcal{S}_e} = L_S \kappa^2 (\nabla v^h \cdot \mathbf{n})^2 \tag{37}$$

$$\|v^h\|^2_{\mathcal{T}_e^-, \kappa} = A^- \kappa |\nabla v^h|^2 \tag{38}$$

  Here, $L_S = \mathrm{meas}(\mathcal{S}_e)$ and $A^- = \mathrm{meas}(\mathcal{T}_e^-)$. As

$$\nabla v^h \cdot \mathbf{n} \leqslant |\nabla v^h| \tag{39}$$

  the generalized inverse estimate (36) is satisfied for

$$C_\mathrm{I}^2 \geqslant \kappa L_S / A^- \tag{40}$$

- *Linear tetrahedron.* Similar to the linear triangle, generalized inverse estimate (36) is satisfied for

$$C_\mathrm{I}^2 \geqslant \kappa A_S / V^- \tag{41}$$

  where $A_S = \mathrm{meas}(\mathcal{S}_e)$ and $V^- = \mathrm{meas}(\mathcal{T}_e^-)$.

DOI: 10.1002/nme

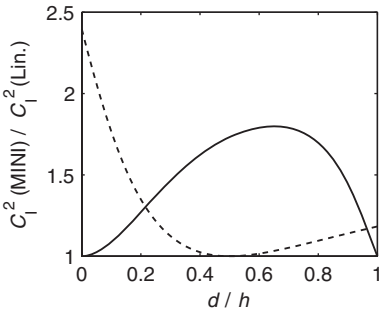

Figure 3. Ratio of constants.

- *Linear triangle with polynomial bubble (the bulk field of a MINI element)* [25]. For practical purposes it is useful to estimate the constant in terms of that of the linear element. Consider a right isosceles triangle of side h, with the interface parallel to one of the sides at a distance d from the element edge. There are two cases: $\mathcal{T}_e^-$ is a trapezoid with area $A^- = (h^2 - d^2)/2$ and $L_S = d$, and $\mathcal{T}_e^-$ is a triangle with area $A^- = (h-d)^2/2$ and $L_S = h - d$. Figure 3 shows the ratio of the lower bound for the constants of the MINI to those of the linear elements for the two cases. Overall, the constant increases with the addition of the bubble, as expected. The largest ratio is $(5+\sqrt{21})/4 \approx 2.4$, for the case of $\mathcal{T}_e^-$ being a triangle as $d/h \to 0$.

Defining the method parameter on the element level in terms of the constant of the generalized inverse estimate (36) as

$$\alpha_e = 2C_{\mathrm{I}}^2 \tag{42}$$

provides coercivity of the bilinear form (cf. (34), (35), (4a), and (8a))

$$a(v^h, v^h)_e = \|v^h\|^2_{\mathcal{T}_e^-,\kappa} - 2\langle \kappa v^h_{,n}, v^h\rangle_{\mathcal{S}_e} + \alpha_e \|v^h\|^2_{\mathcal{S}_e} + \|\beta^{1/2} v\|^2_{\mathcal{T}_e^-} \tag{43}$$

$$\geqslant \|v^h\|^2_{\mathcal{T}_e^-,\kappa} - \varepsilon \|\kappa v^h_{,n}\|^2_{\mathcal{S}_e} + (\alpha_e - 1/\varepsilon)\|v^h\|^2_{\mathcal{S}_e} + \|\beta^{1/2} v\|^2_{\mathcal{T}_e^-} \quad \forall \varepsilon > 0 \tag{44}$$

$$\geqslant (1 - \varepsilon C_{\mathrm{I}}^2)\|v^h\|^2_{\mathcal{T}_e^-,\kappa} + (\alpha_e - 1/\varepsilon)\|v^h\|^2_{\mathcal{S}_e} + \|\beta^{1/2} v\|^2_{\mathcal{T}_e^-} \tag{45}$$

$$= \tfrac{1}{2}\|v^h\|^2_{\mathcal{T}_e^-,\kappa} + \|\beta^{1/2} v\|^2_{\mathcal{T}_e^-} \tag{46}$$

The first line follows from the definition of a, the second line from Young's inequality with ε, the third line from the generalized inverse estimate (36), and last line is obtained by selecting $\varepsilon = 1/\alpha_e$ and $\alpha_e = 2C_{\mathrm{I}}^2$.

Remark
Coercivity is assured with any choice of $\alpha_e \geqslant 1/\varepsilon > C_{\mathrm{I}}^2$. The definition of the parameter (42) provides good performance in computation.

DOI: 10.1002/nme

4.2. Jump condition

The generalized inverse estimate (36) is extended to account for the *average* flux

$$\|\langle \kappa v^h_{,n}\rangle\|_{\mathcal{S}_e} \leqslant C_{\mathrm{I}} \|v^h\|_{\mathcal{T}_e,\kappa} \tag{47}$$

in terms of the energy norm (35).

The lower bound of the constant is estimated for a linear triangle. The gradient is piecewise constant within the element. Assuming that κ is also piecewise constant within each element, the mean flux is constant along the interface; thus,

$$\|\langle \kappa v^h_{,n}\rangle\|^2_{\mathcal{S}_e} = L_S \langle \kappa v^h_{,n}\rangle^2 \tag{48}$$

$$\|v^h\|^2_{\mathcal{T}_e,\kappa} = A^- \kappa^- |\nabla v^{h-}|^2 + A^+ \kappa^+ |\nabla v^{h+}|^2 \tag{49}$$

For the average flux

$$\begin{aligned}
&(\kappa^- \nabla v^{h-} \cdot \mathbf{n} + \kappa^+ \nabla v^{h+} \cdot \mathbf{n})^2 \\
&\quad \leqslant (1+\varepsilon)(\kappa^- \nabla v^{h-} \cdot \mathbf{n})^2 + (1+1/\varepsilon)(\kappa^+ \nabla v^{h+} \cdot \mathbf{n})^2 \quad \forall \varepsilon > 0 && (50)\\
&\quad \leqslant \left(1 + \frac{\kappa^+ A^-}{\kappa^- A^+}\right)(\kappa^-)^2 |\nabla v^{h-}|^2 + \left(1 + \frac{\kappa^- A^+}{\kappa^+ A^-}\right)(\kappa^+)^2 |\nabla v^{h+}|^2 && (51)\\
&\quad = \left(\frac{\kappa^-}{A^-} + \frac{\kappa^+}{A^+}\right)(A^- \kappa^- |\nabla v^{h-}|^2 + A^+ \kappa^+ |\nabla v^{h+}|^2) && (52)
\end{aligned}$$

The first line follows from Young's inequality with ε, and the second line is obtained by selecting $\varepsilon = \kappa^+ A^- / \kappa^- A^+$. For the linear triangle, the generalized inverse estimate (47) is satisfied for

$$C^2_{\mathrm{I}} \geqslant \frac{L_S}{4}\left(\frac{\kappa^-}{A^-} + \frac{\kappa^+}{A^+}\right) \tag{53}$$

Similarly, for the linear tetrahedron, the generalized inverse estimate (47) is satisfied for

$$C^2_{\mathrm{I}} \geqslant \frac{A_S}{4}\left(\frac{\kappa^-}{V^-} + \frac{\kappa^+}{V^+}\right) \tag{54}$$

Defining the method parameter on the element level as before (42), but in terms of the constant of the generalized inverse estimate (47) provides coercivity of the bilinear form

$$\begin{aligned}
a(v^h, v^h)_e &= \|v^h\|^2_{\mathcal{T}_e,\kappa} - 2\langle \langle \kappa v^h_{,n}\rangle, [\![v^h]\!]\rangle_{\mathcal{S}_e} + \alpha_e \|[\![v^h]\!]\|^2_{\mathcal{S}_e} + \|\beta^{1/2} v\|^2_{\mathcal{T}_e} && (55)\\
&\geqslant \|v^h\|^2_{\mathcal{T}_e,\kappa} - \varepsilon \|\langle \kappa v^h_{,n}\rangle\|^2_{\mathcal{S}_e} + (\alpha_e - 1/\varepsilon)\|[\![v^h]\!]\|^2_{\mathcal{S}_e} + \|\beta^{1/2} v\|^2_{\mathcal{T}_e} \quad \forall \varepsilon > 0 && (56)\\
&\geqslant (1 - \varepsilon C^2_{\mathrm{I}})\|v^h\|^2_{\mathcal{T}_e,\kappa} + (\alpha_e - 1/\varepsilon)\|[\![v^h]\!]\|^2_{\mathcal{S}_e} + \|\beta^{1/2} v\|^2_{\mathcal{T}_e} && (57)\\
&= \tfrac{1}{2}\|v^h\|^2_{\mathcal{T}_e,\kappa} + \|\beta^{1/2} v\|^2_{\mathcal{T}_e} && (58)
\end{aligned}$$

Again, the first line follows from the definition of a, the second line from Young's inequality with ε, the third line from the generalized inverse estimate (47), and last line is obtained by selecting $\varepsilon = 1/\alpha_e$ and $\alpha_e = 2C^2_{\mathrm{I}}$. (As noted previously, coercivity is assured with any choice of $\alpha_e \geqslant 1/\varepsilon > C^2_{\mathrm{I}}$, but the definition of the parameter (42) provides good performance in computation.)

DOI: 10.1002/nme

5. NUMERICAL EXAMPLES

We examine a sequence of problems to study the accuracy of the embedded method with the element-level stabilization parameters defined in (40) and (53). We compare results with those obtained using alternative numerical methods for interfacial problems. To evaluate the accuracy in the bulk field, we use the standard L^2 error norm and report normalized, or relative norms. To evaluate the accuracy of the flux on the interface, we use the normalized error norm

$$\mathcal{E}_d(\mathrm{j}^h) := \left(\frac{\int_{\mathcal{S}} (\mathrm{j}^h - \nabla u \cdot \mathbf{n})^2 \, \mathrm{d}\Gamma}{\int_{\mathcal{S}} (\nabla u \cdot \mathbf{n})^2 \, \mathrm{d}\Gamma} \right)^{1/2} \tag{59}$$

where j^h is constructed using domain integrals (30), unless otherwise noted.

For comparison with finite-difference-based methods, we will also find it useful to examine the maximum error at the nodes, which is akin to a sup norm. In particular, we define

$$\|\mathcal{E}_n\|_\infty = \max_{n_i \in \mathcal{R}^h} \{|u(x_i, y_i) - u^h(x_i, y_i)|\} \tag{60}$$

5.1. Planar interface results

Here, we apply the ideas presented above to the following model problem:

$$-\nabla \kappa_1 \nabla u = f \quad \text{in } (0, \mathrm{x}_*) \times (0, 1) \tag{61a}$$

$$-\nabla \kappa_2 \nabla u = f \quad \text{in } (\mathrm{x}_*, 1) \times (0, 1) \tag{61b}$$

$$[\![u]\!] = \bar{\mathrm{i}} \quad \text{at } x = \mathrm{x}_* \tag{61c}$$

$$[\![\kappa \nabla u]\!] \cdot \mathbf{n} = 0 \quad \text{at } x = \mathrm{x}_* \tag{61d}$$

corresponding to a jump-type problem with a planar interface and constant jump $\bar{\mathrm{i}}$ with a zero jump in interfacial flux. The problem is a slight modification of one examined by Hansbo and Hansbo [3]. Choosing $f = 1$ and $\mathrm{x}_* = \frac{1}{2}$, the problem has a simple analytical solution given by

$$u = \begin{cases} \dfrac{(3\kappa_1 + \kappa_2)x}{4\kappa_1^2 + 4\kappa_1\kappa_2} - \dfrac{x^2}{2\kappa_1} & \text{for } 0 \leqslant x \leqslant \dfrac{1}{2} \\ \dfrac{\kappa_2 - \kappa_1 + (3\kappa_1 + \kappa_2)x}{4\kappa_1^2 + 4\kappa_1\kappa_2} - \dfrac{x^2}{2\kappa_2} + \bar{\mathrm{i}} & \text{for } \dfrac{1}{2} \leqslant x \leqslant 1 \end{cases} \tag{62}$$

While this solution only varies in the x-direction, we investigate the problem using two-dimensional meshes.

We report convergence results for this problem based on a series of structured-triangulated meshes, using different choices for κ_1, κ_2, and $\bar{\mathrm{i}}$. The first set of results correspond to $\kappa_2/\kappa_1 = 6$, and $\bar{\mathrm{i}} = 0$. We compare these results with those obtained for the same problem using a standard finite

DOI: 10.1002/nme

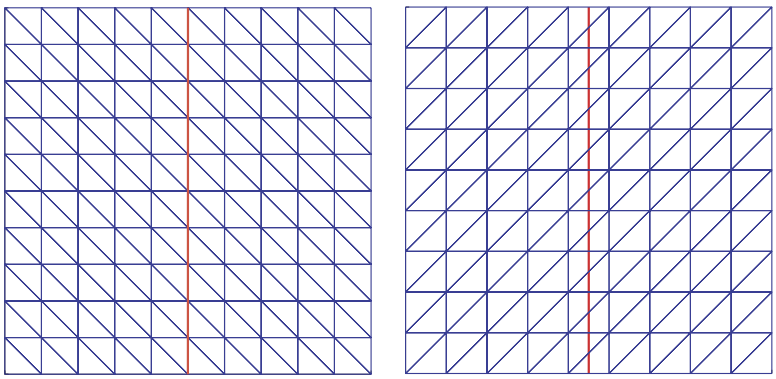

Figure 4. Representative meshes and interface geometry for a standard finite element method (left) and the embedded method (right).

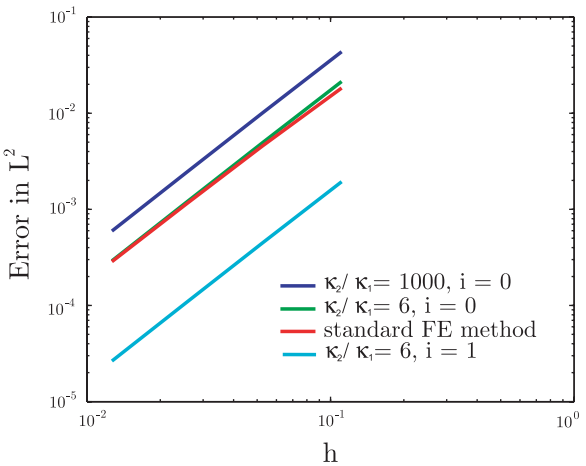

Figure 5. Convergence results obtained using the embedded method for discrete bulk field u^h using various ratios κ_2/κ_1 and interfacial jumps $\bar{\mathrm{i}}$. Results are also shown for a standard finite element method, for the case of $\kappa_2/\kappa_1 = 6$ and $\bar{\mathrm{i}} = 0$.

element method, where the mesh aligns with the interface. Typical meshes for this comparison are shown in Figure 4. The convergence plots shown in Figure 5 indicate quadratic convergence in both cases, with the difference between the results of the embedded and standard methods being indistinguishable. Convergence results for $\kappa_2/\kappa_1 = 1000$ indicate a slight decrease in accuracy, but nonetheless converge at the optimal rate. We likewise report a slight increase in accuracy using $\kappa_2/\kappa_1 = 6$, and $\bar{\mathrm{i}} = 1$. The finite element approximation to the solution in this last case is shown on the coarsest mesh in Figure 6.

DOI: 10.1002/nme

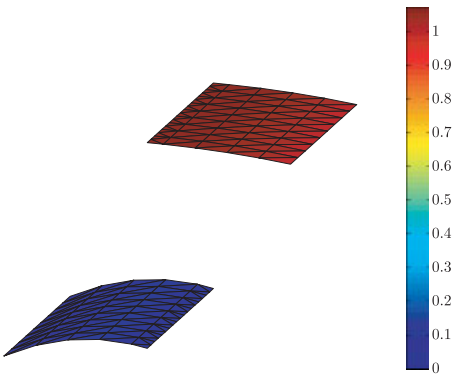

Figure 6. Embedded finite-element approximation to problem (61) with $\kappa_2/\kappa_1 = 6$ and $\bar{\mathrm{i}} = 1$.

We next report results for a model problem studied in Fernandez-Mendez and Huerta [26], Moës *et al.* [15], and our recent work [16, 17]. The bulk and interfacial equations are

$$\Delta u = 0 \quad \text{in } (0,1)\times(\mathrm{y}_*, 1) \tag{63a}$$

$$u = \sin(\pi x)\,\hat{v}(\mathrm{y}_*) \quad \text{at } y = \mathrm{y}_* \tag{63b}$$

$$u = 0 \quad \text{at } y = 1 \tag{63c}$$

$$\nabla u \cdot \mathbf{n}_{\mathrm{o}} = -\pi \hat{v}(y) \quad \text{at } x = 0, 1; \quad \mathrm{y}_* < y < 1 \tag{63d}$$

with known analytical solution (see [26, 27]) given by

$$\hat{u}(x, y) = \sin(\pi x)\hat{v}(y) \tag{64}$$

where $\hat{v}(\bullet) := \cosh(\pi\bullet) - \coth(\pi)\sinh(\pi\bullet)$. In this two-dimensional problem, the embedded interface $\mathcal{S}$ is a horizontal line located at $y = \mathrm{y}_*$, with $0 \leqslant \mathrm{y}_* < 1$. This represents a 'one-sided' Dirichlet-type problem.

We report bulk convergence results (Figure 7) that are optimal and nearly indistinguishable from those using residual-free bubbles [17]. Importantly, the current method is much more efficient than the one employing RFBs, as it does not require one to solve a local system of equations to obtain the element-level stabilization parameter α_e.

We also repeat the sensitivity study examined in [17] for this problem. The basic idea is to examine the accuracy in the approximation to the interfacial flux as the interface position is varied with respect to the underlying mesh. For this purpose, the distance d between $\mathcal{S}$ and the closest (horizontal) row of nodes is varied with respect to the mesh spacing h. The computations are carried out on a structured-triangulated grid with $h = \frac{1}{10}$.

The results of this sensitivity study are shown in Figure 8. We compare the results obtained using the domain-integral method with a direct evaluation of $\nabla u^h \cdot \mathbf{n}$ on the interface, as well as RFB results reported in [17]. The approximate flux obtained from the RFB method is based upon the recovery of a stabilized Lagrange multiplier, given by

$$\lambda^h = \nabla u^h \cdot \mathbf{n} - \alpha_e^{rfb} \int_{\mathcal{S}_e} (u^h - g)\,\mathrm{d}\Gamma \tag{65}$$

DOI: 10.1002/nme

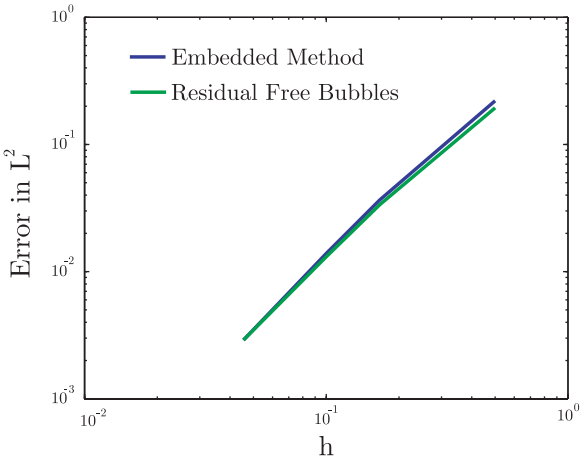

Figure 7. Convergence results for the boundary-value problem (63). Results are shown for the embedded method and the residual-free bubble method proposed by Dolbow and Franca [17].

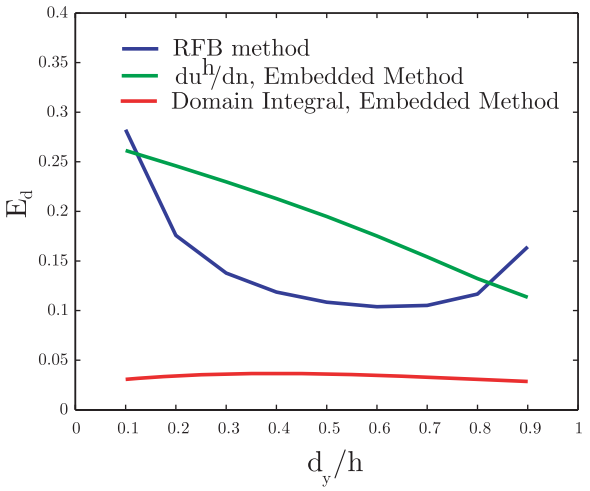

Figure 8. Interfacial error as a function of interface location with respect to the underlying mesh. The distance d_y of the interface from the edge of elements in the mesh is varied.

Clearly, the results obtained using the domain integral exhibit the greatest accuracy and the least amount of sensitivity to interface position. We note that comparable results can be obtained using the domain integral in conjunction with the RFB method as well.

5.2. Curved interface results

In the following examples, a curved interface is considered. In each case, we approximate the interface geometry as the zero iso-contour of an associated implicit function ϕ that is interpolated

DOI: 10.1002/nme

over the underlying finite element mesh. We use a signed distance function to the interface for ϕ, and further approximate the interfacial normal using $\mathbf{n}=\nabla\phi/|\nabla\phi|$.

We first consider a problem described in Vaughan *et al.* [28] on the domain $\mathcal{R}^h=[-1,1]\times[-1,1]$. We define a radial coordinate $r=|\mathbf{x}-\mathbf{x}_c|$ with $\mathbf{x}_c$ the geometric center of the domain. The interface is taken to be a circle with radius $R=\frac{1}{2}$, also centered on the domain. The solution is given by

$$u(x,y)=\begin{cases}1 & r\leqslant\frac{1}{2}\\ 1+\log(2r) & r>\frac{1}{2}\end{cases} \tag{66}$$

We first examine this as a Jump problem given by

$$-\Delta u=0 \quad \text{in } \mathcal{R}^-=\{\mathbf{x}:r<R\} \tag{67a}$$

$$-\Delta u=0 \quad \text{in } \mathcal{R}^+=\{\mathbf{x}:r>R\} \tag{67b}$$

$$[\![u]\!]=0 \quad \text{on } \mathcal{S}=\{\mathbf{x}:r=R\} \tag{67c}$$

$$[\![\nabla u]\!]\cdot\mathbf{n}=-2 \quad \text{on } \mathcal{S}=\{\mathbf{x}:r=R\} \tag{67d}$$

We also employ (66) on the outermost boundary of $\mathcal{R}^h$ as a Dirichlet condition, imposed in the standard manner (i.e. via collocation at the nodes on the boundary).

Using a sequence of both structured and unstructured triangulations, we report optimal rates of convergence in the L^2 norm of the error for this problem. The approximation to the solution over a uniform, but unstructured mesh is shown in Figure 9. It is also interesting to examine the rate of convergence in the sup norm (60) for this problem (Figure 10). In this case, we report results that are nearly indistinguishable from those reported for the X-FEM in Vaughan *et al.* [28] and those reported for the immersed interface method in Beale *et al.* [29]. The three methods appear to give much more accurate results than those obtained with the ghost fluid method for the same problem as reported by Liu *et al.* [22]. We note that the immersed interface and ghost fluid methods are based on finite-difference stencils that are modified in the vicinity of the interface.

There are a few points that bear emphasis here. First, the results of Vaughan *et al.* [28] were obtained using Heaviside enrichment over structured grids of bilinear quadrilateral elements.

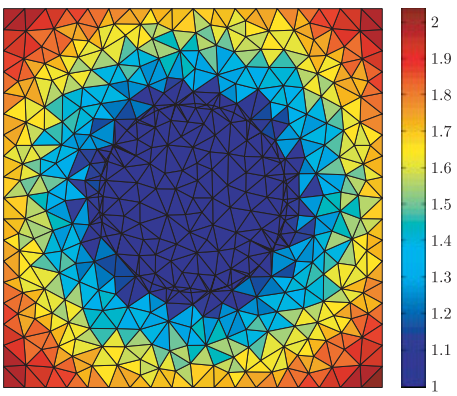

Figure 9. Finite element approximation to solution to circular-interface problem (67).

DOI: 10.1002/nme

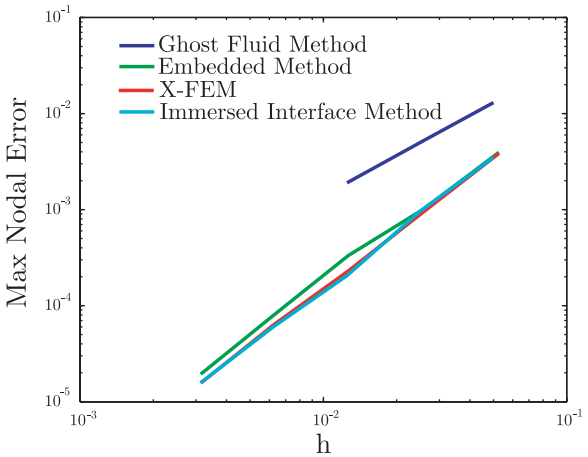

Figure 10. Convergence results in the maximum nodal error for the embedded finite element method compared with results reported in Liu *et al.* [22], Vaughan *et al.* [28], and Beale *et al.* [29].

It is, therefore, interesting that we obtain comparable results over unstructured grids using elements with slightly lower precision. Second, we note that the method is much more efficient than that of Vaughan *et al.* [28], as it does not rely on an additional Lagrange multiplier field to enforce the interfacial constraints.

We next examine this as the Dirichlet problem given by

$$-\Delta u = 0 \quad \text{in } \mathcal{R}^- = \{\mathbf{x} : r < R\} \tag{68a}$$

$$-\Delta u = 0 \quad \text{in } \mathcal{R}^+ = \{\mathbf{x} : r > R\} \tag{68b}$$

$$u^+ = 1 \quad \text{on } \mathcal{S} = \{\mathbf{x} : r = R\} \tag{68c}$$

$$u^- = 1 \quad \text{on } \mathcal{S} = \{\mathbf{x} : r = R\} \tag{68d}$$

The results of the convergence study are shown in Figure 11. We report optimal rates of convergence in the bulk and interfacial fields with the embedded method. It is interesting to note that, as compared with the analogous jump problem (67), slightly better accuracy in the bulk error norms is obtained.

As a last example of a curved, stationary interface problem, we consider the Jump problem given in Liu *et al.* [22], where the interface geometry is defined by the collection of points

$$\begin{aligned} X &= 0.02\sqrt{5} + (0.5 + 0.2\sin(5\theta))\cos(\theta) \\ Y &= 0.02\sqrt{5} + (0.5 + 0.2\sin(5\theta))\sin(\theta) \end{aligned} \qquad -\pi \leqslant \theta < \pi \tag{69}$$

on the domain $\mathcal{R} = [-1.0, 1.0] \times [-1.0, 1.0]$. The interior region is taken as $\mathcal{R}^-$, and the governing equations and jump conditions are given by:

$$-\kappa^- \Delta u = -4 \quad \text{in } \mathcal{R}^- \tag{70a}$$

$$-\kappa^+ \Delta u = -16(x^2 + y^2) \quad \text{in } \mathcal{R}^+ \tag{70b}$$

DOI: 10.1002/nme

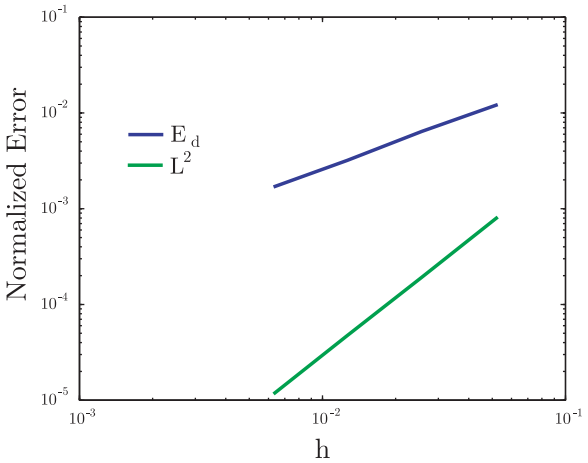

Figure 11. Convergence results for bulk and interfacial fields for the circular interface problem (68), using the embedded method.

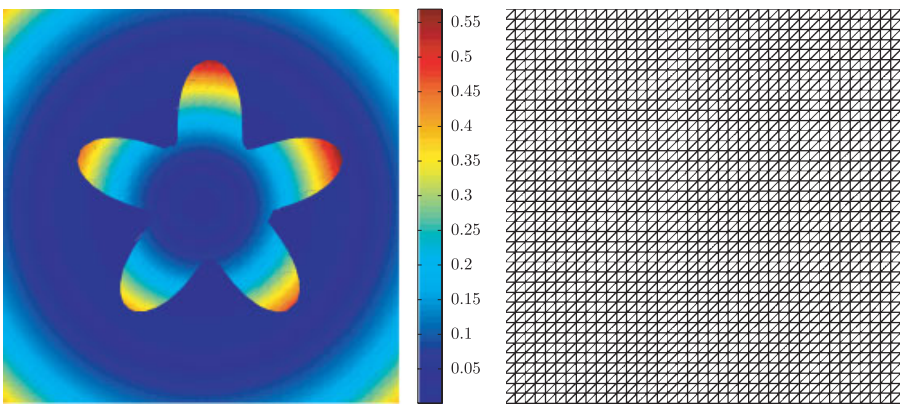

Figure 12. Finite element approximation to solution of curved interface problem (70) (left) over structured-triangulated mesh (right).

$$[\![u]\!] = 0.1(x^2+y^2)^2 - 0.01\log(2\sqrt{x^2+y^2}) - (x^2+y^2) \quad \text{on } \mathcal{S} \tag{70c}$$

$$[\![\kappa\nabla u]\!]\cdot\mathbf{n} = (4(x^2+y^2) - 0.1(x^2+y^2)^{-1} - 2)(xn_1+yn_2) \quad \text{on } \mathcal{S} \tag{70d}$$

Taking $\kappa^- = 1$ and $\kappa^+ = 10$, the solution is

$$u(x,y) = \begin{cases} x^2+y^2 & (x,y)\in\mathcal{R}^- \\ 0.1(x^2+y^2)^2 - 0.01\log(2\sqrt{x^2+y^2}) & (x,y)\in\mathcal{R}^+ \end{cases} \tag{71}$$

The embedded interface approximation over a typical structured mesh is shown in Figure 12.

DOI: 10.1002/nme

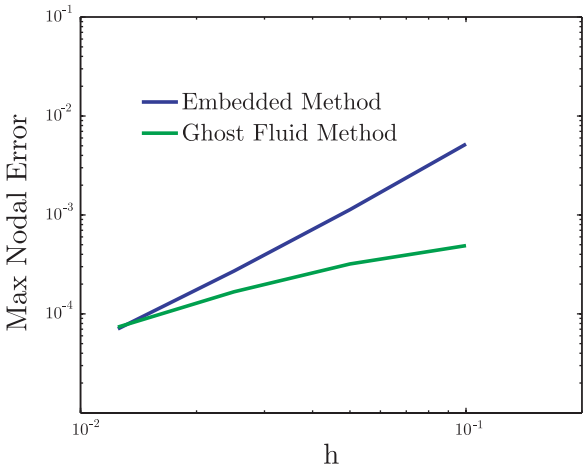

Figure 13. Comparison in convergence in max nodal error for the curved interface problem (70) using the embedded method and the ghost fluid method of Liu *et al.* [22].

We report optimal rates of convergence for this problem using the embedded method. We compare the max nodal error using the embedded method with the results reported by Liu *et al.* [22] for the same problem. These convergence results are given in Figure 13. While not as accurate over coarse meshes, the embedded method exhibits a superior rate of convergence and eventually matches the accuracy of the ghost fluid method.

5.3. Evolving interface example

We now apply the embedded interface method to simulate an evolving interface problem. In particular, we consider the simulation of resin transfer molding (RTM), in which a low-viscosity resin is injected into a mold containing a porous reinforcement material. The problem can be idealized using Darcy's law, which assumes that the fluid velocity $\mathbf{v}_d$ is proportional to the pressure gradient

$$\mathbf{v}_d = -\frac{\boldsymbol{\kappa}}{\mu} \cdot \nabla p \tag{72}$$

where $\boldsymbol{\kappa}$ denotes the permeability and μ the dynamic viscosity. The effective particle velocity $\mathbf{v}_e$ in the resin is related to the Darcy velocity $\mathbf{v}_d$ through

$$\mathbf{v}_e = \frac{\mathbf{v}_d}{\phi} \tag{73}$$

where ϕ is the porosity. Assuming that both $\boldsymbol{\kappa}$ and μ are constant, conservation of mass implies an elliptic equation for the pressure, i.e.

$$\Delta p = 0 \tag{74}$$

If one is only interested in the free-surface velocity of the mold, a relatively simple procedure can be employed. This amounts to finding the pressure field that satisfies (74) in the mold domain, and evaluating the effective velocity at the free surface through (73) and (72).

DOI: 10.1002/nme

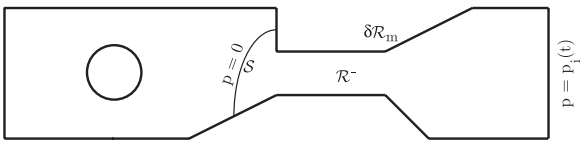

Figure 14. Geometry used in resin transfer molding simulation. The pressure is specified as a function of time at the inlet boundary on the right, and fixed to zero on the evolving resin front $\mathcal{S}$. The other boundaries are flux-free, see Moës *et al.* [15] for precise dimensions.

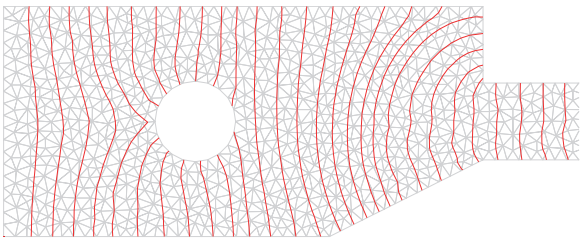

Figure 15. Successive flow front positions (solid lines) and background mesh (gray) in resin transfer molding simulation, in the vicinity of the hole.

We follow the work of Moës *et al.* [15] and use this approach to simulate RTM in the geometry shown in Figure 14. We use $\mathcal{R}^-$ to denote the portion of the mold occupied by the resin. The pressure at the inlet varies with time and is prescribed according to experimental measurements. The pressure at the free surface of the resin, which we take as $\mathcal{S}$, is fixed at zero. Perfect slip is assumed where the resin meets the walls of the mold, which translates into flux-free boundary conditions for the Laplace equation (74). The material properties employed for the simulation are: $\mu = 0.1\,\text{Pa s}$, $\boldsymbol{\kappa} = K\mathbf{I}$, with $K = 5.2 \times 10^{-10}\,\text{m}^2$ and $\phi = 0.71$.

To evolve the geometry of the front, we use the level set method with the assumed gradient finite element formulation described in Mourad *et al.* [30]. We use the second-order, lumped-mass algorithm. The time step is set by the CFL condition and the maximum extension velocity, and we redistance the level set function according to the criteria proposed by Mourad *et al.* [30]. The background mesh is held fixed, and the embedded method outlined in Section 3 is used to enforce the condition at the free surface of the resin.

A zoom of the front geometry near the hole at various time steps is shown superimposed over the background mesh in Figure 15. These results correspond to extension velocity fields constructed based on fluxes obtained from the domain-integral method, using (30) and (33). We note good qualitative comparison with the results of Moës *et al.* [15]. The simulated front evolves monotonically and as smoothly as the mesh can accommodate.

Interestingly, we obtain comparable results even using the less-accurate direct evaluation of the normal pressure gradient $\partial p^h / \partial \mathbf{n}$ to construct the extension velocities. These results indicate a surprising robustness for the method. Figure 16 shows an excellent comparison of the experimental and simulated front positions using both extension velocity fields as a function of time. The experimental results are identical to those presented in Moës *et al.* [15].

DOI: 10.1002/nme

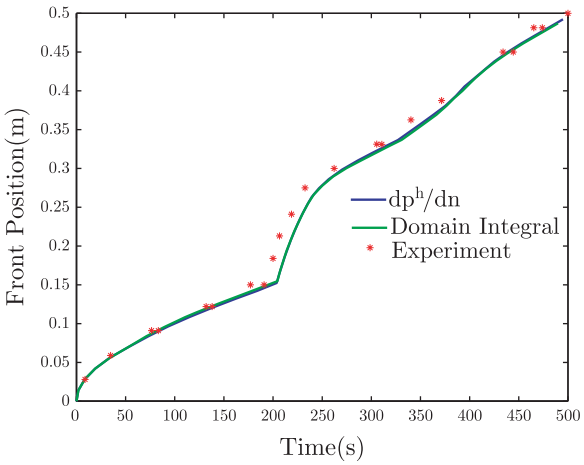

Figure 16. Comparison of numerical predictions and experimental measurements of resin front position as a function of time. Results are shown for extension velocities using approximate interfacial fluxes obtained from the domain-integral method and the normal pressure gradient $\partial p^h/\partial \mathbf{n}$ on the interface.

6. SUMMARY AND CONCLUDING REMARKS

This work presents an efficient finite element method for embedded interface problems. We develop the method for two different classes of interfacial conditions, corresponding to jump and Dirichlet problems. In each case, the starting point is a variational form that seeks to impose interfacial conditions weakly, employing Nitsche's method for stabilization. In the vicinity of the interface, discretization is based on the use of overlapping finite elements, akin to enrichment with the Heaviside function in the X-FEM. This construction allows the approximation to capture discontinuities in both the primary field and its gradient across the interface. Suitable choices for the interfacial stabilization terms are provided by numerical analysis, in particular by insisting on the coercivity of the discrete bilinear form. The method is straightforward to implement, requiring only the modification of element stiffness routines for elements intersected by the interface. Numerical studies indicate that the accuracy of the method is competitive with existing methods for elliptic interface problems, over both structured and unstructured meshes.

The efficiency of the method stems from a number of considerations. The method does not rely on an additional Lagrange multiplier field to enforce interfacial constraints. The stabilization parameters are obtained via algebraic expressions at the element level, rather than calculations based on residual-free bubbles. In comparison to enrichment with the ridge function to capture slope discontinuities, the discretization employed by the embedded method does not increase the order of the basis functions. As a result, the same order quadrature rule that is employed in elements away from the interface can also be used in elements intersected by the interface, modulo the usual adjustments. For linear elements and simple Poisson problems, this amounts to little more than scaling the standard element stiffness matrices by the percentage of the element domain on each side of the interface. We contend that for jump problems (or those with 'weak' discontinuities), the resulting method is more efficient and easier to implement than enrichment with the ridge function or the use of blending [12, 13].

DOI: 10.1002/nme

Going forward, a number of obvious extensions for the method can be envisioned. The extension to three-dimensional problems, employing the estimates (41) and (54) for stabilization terms, is work in progress. Transient problems are also of interest, with algorithmic issues associated with time-stepping having received relatively little attention for methods with enriched discretizations. Finally, we mention problems in which the bilinear form is not self-adjoint, such as incompressible fluid flow. Techniques for stabilizing interfacial constraints in conjunction with bulk constraints (such as volumetric incompressibility) remain to be examined thoroughly.

ACKNOWLEDGEMENTS

The support of the Air Force Office of Scientific Research and the Department of Energy to Duke University is gratefully acknowledged.

REFERENCES

1. Moës N, Dolbow J, Belytschko T. A finite element method for crack growth without remeshing. *International Journal for Numerical Methods in Engineering* 1999; **46**(1):131–150.
2. Daux C, Moës N, Dolbow J, Sukumar N, Belytschko T. Arbitrary branched and intersecting cracks with the extended finite element method. *International Journal for Numerical Methods in Engineering* 2000; **48**(12): 1741–1760.
3. Hansbo A, Hansbo P. An unfitted finite element method, based on Nitsche's method, for elliptic interface problems. *Computer Methods in Applied Mechanics and Engineering* 2002; **191**:5537–5552.
4. Zhang LT, Gerstenberger A, Wang X, Liu W. Immersed finite element method. *Computer Methods in Applied Mechanics and Engineering* 2004; **193**:2051–2067.
5. Moës N, Cloirec M, Cartraud P, Remacle JF. A computational approach to handle complex microstructure geometries. *Computer Methods in Applied Mechanics and Engineering* 2003; **192**:3163–3177.
6. Merle R, Dolbow J. Solving thermal and phase change problems with the extended finite element method. *Computational Mechanics* 2002; **28**(5):339–350.
7. Chessa J, Smolinski P, Belytschko T. The extended finite element method for solidification problems. *International Journal for Numerical Methods in Engineering* 2002; **53**(14):1959–1977.
8. Dolbow JE, Fried E, Ji H. A numerical strategy for investigating the kinetic response of stimulus-responsive hydrogels. *Computer Methods in Applied Mechanics and Engineering* 2005; **194**:4447–4480.
9. Ji H, Chopp DL, Dolbow J. A hybrid extended finite element level set method for modeling phase transformations. *International Journal for Numerical Methods in Engineering* 2002; **54**:1209–1233.
10. Duddu R, Bordas S, Chopp D, Moran B. A combined extended finite element and level set method for biofilm growth. *International Journal for Numerical Methods in Engineering* 2008; **74**(5):848–870.
11. Nitsche JA. Über ein Variationsprinzip zur Lösung von Dirichlet-Problemen bei Verwendung von Teilräumen, die keinen Randbedingungen unterworfen sind. *Abhandlungen aus dem Mathematischen Seminar der Universität Hamburg* 1970–1971; **36**:9–15.
12. Gracie R, Wang HW, Belytschko T. Blending in the extended finite element method by discontinuous Galerkin and assumed strain methods. *International Journal for Numerical Methods in Engineering* 2008; **74**(11):1645–1669.
13. Fries TP. A corrected XFEM approximation without problems in blending elements. *International Journal for Numerical Methods in Engineering* 2008; **75**(5):503–532.
14. Ji H, Dolbow JE. On strategies for enforcing interfacial constraints and evaluating jump conditions with the extended finite element method. *International Journal for Numerical Methods in Engineering* 2004; **61**(14): 2508–2535.
15. Moës N, Béchet E, Tourbier M. Imposing essential boundary conditions in the extended finite element method. *International Journal for Numerical Methods in Engineering* 2006; **67**(12):1641–1669.
16. Mourad HM, Dolbow J, Harari I. A bubble-stabilized finite element method for Dirichlet constraints on embedded interfaces. *International Journal for Numerical Methods in Engineering* 2007; **69**:772–793.
17. Dolbow JE, Franca LP. Residual-free bubbles for embedded Dirichlet problems. *Computer Methods in Applied Mechanics and Engineering* 2008; **197**(14):3751–3759.

DOI: 10.1002/nme

18. Carey GF, Chow SS, Seager MK. Approximate boundary-flux calculations. *Computer Methods in Applied Mechanics and Engineering* 1985; **50**:107–120.
19. Areias PMA, Belytschko T. A comment on the article 'A finite element method for simulation of strong and weak discontinuities in solid mechanics' by A. Hansbo and P. Hansbo. *Computer Methods in Applied Mechanics and Engineering* 2006; **195**(9–12):1275–1276.
20. Song JH, Areias PMA, Belytschko T. A method for dynamic crack and shear band propagation with phantom nodes. *International Journal for Numerical Methods in Engineering* 2006; **67**(6):868–893.
21. Melenk J, Babuška I. The partition of unity method: basic theory and applications. *Computer Methods in Applied Mechanics and Engineering* 1996; **139**:289–314.
22. Liu XD, Fedkiw RP, Kang M. A boundary condition capturing method for Poisson's equation on irregular domains. *Journal of Computational Physics* 2000; **160**:151–178.
23. Barbosa HJC, Hughes TJR. The finite element method with Lagrange multipliers on the boundary: circumventing the Babuška–Brezzi condition. *Computer Methods in Applied Mechanics and Engineering* 1991; **85**(1):109–128.
24. Stenberg R. On some techniques for approximating boundary conditions in the finite element method. *Journal of Computational and Applied Mathematics* 1995; **63**:139–148.
25. Arnold DN, Brezzi F, Fortin M. A stable finite element for the Stokes equations. *Calcolo* 1984; **21**(4):337–344.
26. Fernandez-Mendez S, Huerta A. Imposing essential boundary conditions in mesh-free methods. *Computer Methods in Applied Mechanics and Engineering* 2004; **193**:1257–1275.
27. Wagner GJ, Liu WK. Hierarchical enrichment for bridging scales and mesh-free boundary conditions. *International Journal for Numerical Methods in Engineering* 2001; **50**(3):507–524.
28. Vaughan BL, Smith BG, Chopp DL. A comparison of the extended finite element method with the immersed interface method for elliptic equations with discontinuous coefficients and singular sources. *Communications in Applied Mathematics and Computational Science* 2006; **1**:207–228.
29. Beale JT, Chopp D, Leveque RJ, Li Z. Correction to: a comparison of the extended finite element method with the immersed interface method for elliptic equations with discontinuous coefficients and singular sources. *Communications in Applied Mathematics and Computational Science* 2008; **3**:95–100.
30. Mourad HM, Dolbow J, Garikipari K. An assumed gradient finite element method for the level set equation. *International Journal for Numerical Methods in Engineering* 2005; **64**:1009–1032.

DOI: 10.1002/nme